



SAN CARLOS DIVISION

990 COMMERCIAL ST., SAN CARLOS, CA 94070-4084
TELEPHONE (415) 595-1100 TWX 910 376 4409

QUANTIC INDUSTRIES, INC.

NOTICE: THIS DOCUMENT CONTAINS PROPRIETARY INFORMATION WHICH IS THE EXCLUSIVE PROPERTY OF QUANTIC INDUSTRIES, INC. AND MAY NOT BE REPRODUCED IN WHOLE OR IN PART, OR USED FOR THE MANUFACTURING OF PARTS WITHOUT THE WRITTEN PERMISSION OF THE OWNERS.

ER-817
PHASE I FINAL REPORT
Long-Life 3-Axis Satellite Attitude Sensing

Contract NAS5-30055

31 August 1987

Submitted to: NASA Goddard Space Flight Center
ATTN: Rosa Acevedo, Code 287
Greenbelt, MD 20771

Prepared by:

Tor Arild
Senior Opto-Mechanical Engineer

Approved by:

E. W. Morales
Vice President, Engineering
San Carlos Division



ACKNOWLEDGEMENTS

This document was authored by the following individuals:

Oliver Edwards, *Optical Design and Theory*

Tor Arild, *Mechanical Design*

Ed Rose, *Electronic Design*

Gerhard Batke, *Manufacturing*

CONTRACT NAS5-30055
PHASE I PROJECT SUMMARY

The purpose of this research was to investigate the feasibility of new, moderate-cost, high reliability navigation sensors for high-altitude satellites, using stellar sources to obviate the use of gyroscopic devices.

Based on consultations with cognizant NASA personnel and the Program Office at the start of the effort, the primary investigation focused on the need for developing a new star tracker model to replace an old star tracker which is still needed for current probe and satellite programs.

One innovative element of the proposed star tracker was the design, development, and testing of technology components related to a "phase scrambler plate" as described in the Phase I proposal. The purpose of the phase scrambler plate is to convert the impulse response of the optical system from a point image to a uniformly bright, square, angularly large ($1^\circ - 2^\circ$), in-focus image of the star source. Conventional quad-cell or CCD array star trackers operate defocused to create a large focal spot. Not only does this make them very sensitive to mechanical and thermal stresses, but they suffer from large nonlinearities as the nonuniform circular star image traverses the cruciform dividing lines of the array. As a result of obtaining the uniform, large-angle, square impulse response, it becomes possible to obtain accurate, stable, linear off-axis tracking using a conventional quad-cell signal-balance system.

The phase scrambler plate appears to be a unique and patentable combination of technology, and a patentability search is being performed.

A collimated star source was built and tested. A breadboard star tracker with an $8^\circ \times 8^\circ$ field of view was designed and built. It was tested in normal quad-cell mode (without the phase scrambler plate) and with the phase scrambler plate. Although the phase scrambler plate was crudely made (as a first demonstration), the performance of the star tracker breadboard was greatly improved using the phase scrambler plate, instead of system defocus.

If further developed, the phase scrambler plate may be added as a low-cost retroconversion to any objective lens to greatly improve quad-cell or CCD array tracking; applications include star trackers, laser metrology, laser machining optics, and surveying instrumentation.



LONG-LIFE 3-AXIS SATELLITE ATTITUDE SENSING
CONTRACT NAS5-30055
PHASE I FINAL REPORT

1.0 INTRODUCTION

Quantic's Phase I proposal described a variety of technical approaches for eliminating moving parts (gyroscopes) from satellite attitude sensors to permit a longer system life. These potential solutions included earth sensors, a proprietary yaw sensor, and low-cost star (Polaris, Canopus) trackers.

An initial post-award review with cognizant NASA personnel redirected the program toward the development of a low-complexity, high-reliability star tracker to support a number of on-going probe and satellite guidance programs.

The proposed star tracker is a large-area quad-cell array tracker. The key technology for increasing the reliability and accuracy of quad-cell tracking was Quantic's development of the "phase scrambler plate"--an optical element incorporated into the objective lens to tailor the lens' impulse response. The phase scrambler plate can change a star image from a circular Airy disc into a uniformly-filled square, circle, line, or other desired image shape. The dimensions of the image may be tailored to any desired size. In the present experiment, a 0.01° Gaussian star image was transformed into a $2^\circ \times 2^\circ$ uniformly bright square image.

The principles of servo-balance tracking are broadly applied to quad-cell tracking and to the CCD and CID star mappers instruments. In star mappers, moments are calculated to locate the centroid of the star image within a 2×2 or (e.g.) a 6×6 cell array. The linearity of such devices has periodic error, limited by the convolution of a circular Gaussian spot with a square detector array.

In contrast, Quantic's phase scrambler plate yields a square uniform focal spot. Angular measurements of the image motion across a quad-cell or CCD/CID array are essentially linear, across the full field of view.

Expanding the image to fill a quad-cell array has in the past usually been accomplished by gross defocus of the system, making the system readout accuracy extremely sensitive to small thermal or mechanical shifts in its structural components. The phase scrambler plate permits the system to be operated at "best focus", with a resultant large tolerance for mechanical and thermal changes.

Research carried out included optimization of the phase scrambler plate design, fabrication of a phase scrambler plate and its incorporation into a 4×4 inch square objective lens, fabrication and successful testing of a breadboard star tracker with an $8^\circ \times 8^\circ$ field of view.

Potential applications of this research are to obtain a significant improvement in the linearity (accuracy), robustness, and reliability of quad-cell or CCD/CID array star trackers, theodolites, laser machining optics, or surveying instruments. At the same time, the simplified lens design may greatly decrease manufacturing costs.



2.0 STATEMENT OF THE PROBLEM

In its initial SBIR Request for Quotations, NASA sought (under Topic 9.03) investigations leading to a gyro-less, 3-axis attitude sensor system for geosynchronous orbit.

Gyro failure is generally a catastrophic failure. A moving-rotor gyro may be required to make on the order of 10^{10} revolutions in its life; this is not an intrinsically comforting approach to building critical navigation instrumentation.

In an approach to obviating the need for gyroscopes, Quantic proposed to use Earth and/or star references, updated at a frequency which is small compared to the frequency of drift and correction motions.

An initial post-award review with cognizant NASA personnel added the following notes:

- Gyro breakdown is rarely a limitation to satellite life.
- The yaw sensor will not separate roll rate from yaw error angle, and hence exhibits a crosscoupling effect. Since the proposed yaw sensor is not independent of roll, existing gyro-compassing systems are adequate. The earlier proposed system thus would have limited attraction in a similar application.
- An immediate and serious problem exists in the dwindling stock of star trackers left from an earlier NASA probe program. These available image-dissector star trackers have been used to support current probe and satellite programs, but few remain. A critical need has been perceived for a low-cost, moderate-accuracy Polaris star tracker to be developed for reliable small-volume manufacture.

Hence, the problem to be addressed became attitude sensing as follows:

- Pitch and roll angles may be readily obtained from Earth sensors. Quantic and others have developed infra-red horizon sensors since the dawn of the space age, and further development is not contemplated under this program.
- Stabilization data from a third axis is to be obtained. As proposed, a Quantic-developed sensor will directly supply the yaw error angle, except that roll rate and yaw angle are not independently measured.

An alternate source of third-axis data would be a Polaris, Canopus, or general star tracker. As a result, a preferred task for this program is to investigate the design of a star tracker as originally proposed.

Desiderata for this star tracker include:

- *Low cost.* If the star tracker can be made sufficiently simple, robust, self-calibrating, and maximally uses off-the-shelf technology and components, then it is reasonable to set as a comparative goal the marginal cost of a conventional Sun tracker.



- *High reliability.* If the optics, detectors, and analytic electronics can be made sufficiently simple, then the MTBF of the star tracker should approach that of a conventional Sun tracker.
- *Off-the-shelf technology.* A new design of star tracker should preferably not involve untried principles or new principles of physics, although novel combinations of proven technology may be required.
- *Off-the-shelf components.* A major problem with many otherwise desirable technologies is that the manufacture of the components themselves is difficult for NASA to use. For example, "standardizing" on any one CCD has been very frustrating: the long and expensive product testing and approval cycle required by NASA for space-qualification has proven to exceed the lives of the product lines in the market, or of the manufacturers themselves. The star tracker should accomplish its tasks using simple components which are already available in space-qualified manufacture or are easily qualified.
- *Functional replacement for the "Fine Guidance Error Sensor" (FGES).* Designed for use on sounding rockets many years ago, a dwindling number of star trackers have been available for moderate-cost missions at NASA Goddard. In the intervening time, these have nearly been consumed, and a specific need exists for their replacement.

Some operational data on the FGES include:

Field of view: 8° diameter
 Weight: 11.5 lb.
 Size: 5 " diameter by 11.5" long
 Power input: 10 watt average
 Selectable fields of view: 2°, 4°, 8°
 Null accuracy: ± 1 arc min.
 Star magnitude detected: -0.5 to +4 m

The primary problem to be addressed in Phase I of the program was to test the principles of Quantic's phase scrambler plate, to implement it in a breadboard star tracker system, to build a collimated star source, and to test the integrated system.

3.0 THEORY OF PHASE SCRAMBLER PLATE (PSP)

Used alone, a conventional objective lens brings all the rays traversing its aperture to a "point" at best focus. Actually, of course, the focal spot has an angular width of $2.44 \frac{\lambda}{A}$ where λ = wavelength of light and A = aperture of the lens. The PSP divides the aperture of the lens into a number of sub-apertures, and places a different prism in front of each sub-aperture to deflect the principle ray of the sub-aperture to a specific angular location.



The focal spots of the sub-apertures are "stacked up" by the prisms to cover the desired spot size and shape, and the number of sub-apertures is varied to ensure a uniform fill between adjacent spots. As is apparent in the above equation, the diffraction-limited width of the focal spot is inversely proportional to the sub-aperture diameter (d).

This is discussed in greater detail as follows.

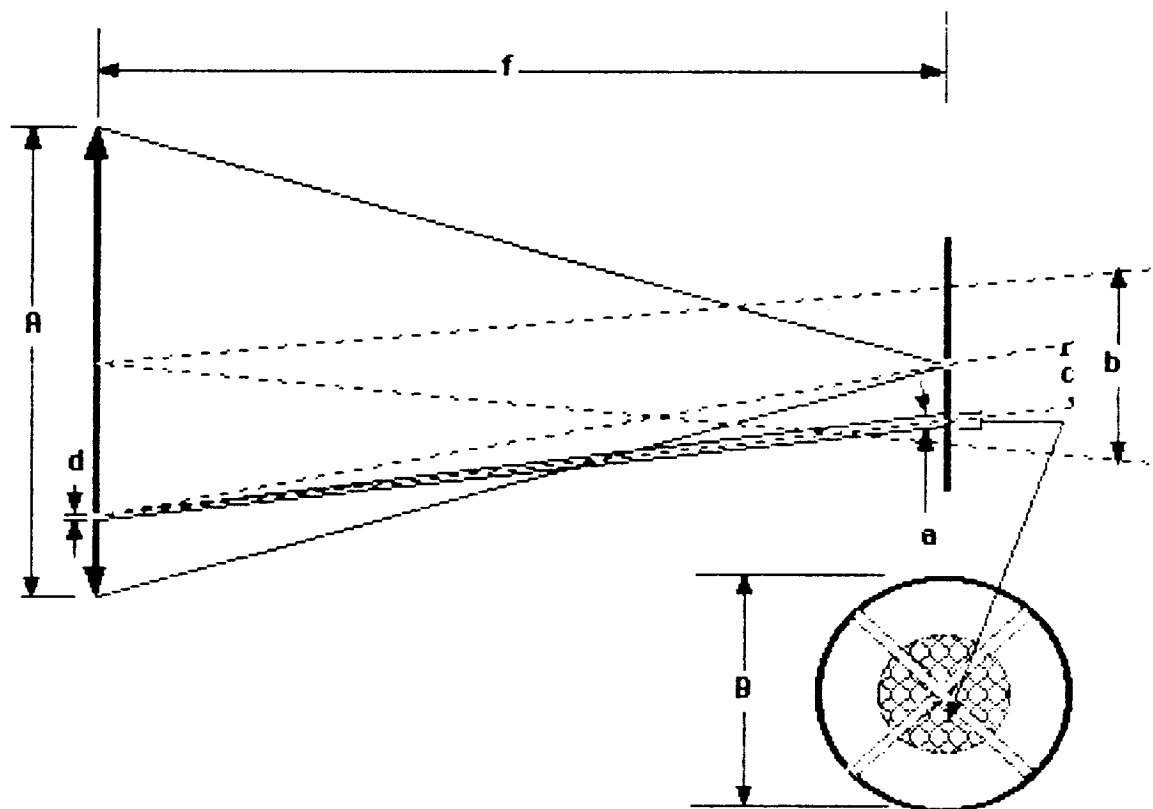


Figure 1. Radiometer With Phase Scrambler Plate.

When using a round quad cell, the ideal spot diameter is half of the cell width. For a quad cell as shown above of total width B (e.g., the inner cell of the concentric cell array of the Polaris tracker), the ideal point-source image spot is a uniformly illuminated disc, $B/2$ in diameter, having an angular width from the lens of $b = B/f$.

Let a small aperture (pinhole) of diameter d be introduced in the aperture of a lens of diameter A.

The diffraction-limited angular width of the first minimum of the Airy disc will be:

$$a = 2.44 \frac{\lambda}{d}$$

If a second such focal spot, mutually incoherent, is now placed beside the first, but whose center is removed by an angle $s = a/2$, the contiguous spots will satisfy the condition of the Rayleigh criterion of telescopic resolution: the maximum of one Airy disc falls on the first minimum of the second.



Unfortunately, for Rayleigh-criterion-separated focal spots the summed illumination in the space between them is not constant: it dips to a minimum of 86% of either maximum, permitting the two images to be easily "resolved," as illustrated in Figure 2.

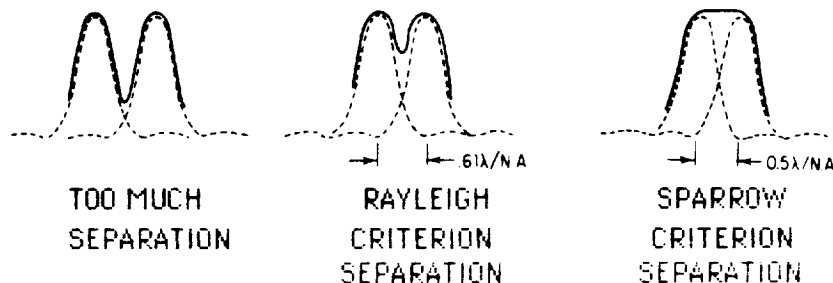


Figure 2. Effects of Increasing the Number (Decreasing the Diameter) of Sub-Apertures.

For the case of smooth, "flat" illumination of the image plane, the Sparrow criterion should be used. For this criterion the angular separations between centers of contiguous spots is:

$$s = \frac{\lambda}{d}$$

If such focal spots are stacked across a diameter to assemble a uniformly illuminated disc image, then a quantity (b/s) of them will be required.

If a method could be devised for mapping the aperture points one for one into the image plane, then an identical number of small pinholes of diameter d would be required across the aperture diameter A. In fact, this is an approximate equality: a higher density of aperture pinholes mapped into overlapping spots in the image plane will only improve the uniformity of illumination.

This condition requires that:

$$\frac{A}{d} \geq \frac{b}{s} \quad \text{or} \quad d^2 \leq \frac{A\lambda}{b}$$

For the example of a 4-inch aperture star tracker ($A = 4"$) using a 4° wide quad cell ($b=2^\circ$), and using $\lambda = 0.55 \mu$, then $d \leq .0498$ inch. For comparison, 18 gage wire is .0475 in diameter.



The effect of aperture on maximum size of sub-aperture for a 2° uniformly illuminated spot follows.

Aperture Diameter A (in.)	Maximum Diameter d (in.)	Total Number of Sub-Apertures (N)
3	.0431	3805
4	.0498	5067
5	.0557	6331
6	.0610	7598

For this irradiation summation to create a disc of uniform illumination in the image plane,

- i) the aperture A is divided into sub-apertures of diameter d, and
- ii) the corresponding focal spots are mutually incoherent, at least with respect to their nearest neighbors in the image plane, and
- iii) the regions of the aperture are piecewise mapped onto the image plane: each region of the aperture "takes up" an equal fraction of the area of the image plane. In the simplest case, the aperture and the image plane are each divided into geometrically similar, uniformly spaced sub-apertures (such as a hexagonal or checkerboard array) and each region of the image contains a uniform array of focal spots.

There is no problem with scrambling the mapping: i.e. nothing requires that the rays from one sub-aperture not cross those on another on the way to the image plane.

MAPPING FUNCTION: DIRECTING THE FOCAL SPOTS FROM EACH SUB-APERTURE

In an aberration-free lens, the rays (from an on-axis point source) through each point of the aperture converge toward the on-axis image of the source. In Figure 1 above, we see that the ray bundle from the sub-aperture has somehow been diverted by an angle "c."

By inspection, we can see that if c is proportional to the radial location of the sub-aperture, then the focal spots from each sub-aperture will be assembled in a uniform array at the focal plane--at least within the small-angle approximations and for Gaussian optics.

This is one of an infinite number of possible and equally effective mapping functions. This one has a particularly simple method of physical implementation and manufacture that is discussed below.



As shown in Figure 3A, a thin prism of apex angle P deflects a ray by an angle $D = P(n-1)$, where n = index of refraction of the prism material. In order to map an element of the aperture into an equivalent element of the image, we wish to have $D \propto R$ where R = local radius of the lens aperture (or of the image). In this case, each element of the aperture is mapped in one-to-one correspondence onto the image element.

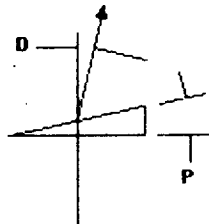


Figure 3A. Thin Prism.

Thus we want the prism apex angle P proportional to R (or " g "), its distance from the optic axis. I.e., the slope of the surface increases linearly from the axis to the periphery.

For a rotationally symmetric lens, this is the defining property of a spherical surface, as shown in Figure 3B, given that the slope increases along every radius. For a single dimension, this defines a cylindrical surface given that the slope increases along the width (but is zero along the length).

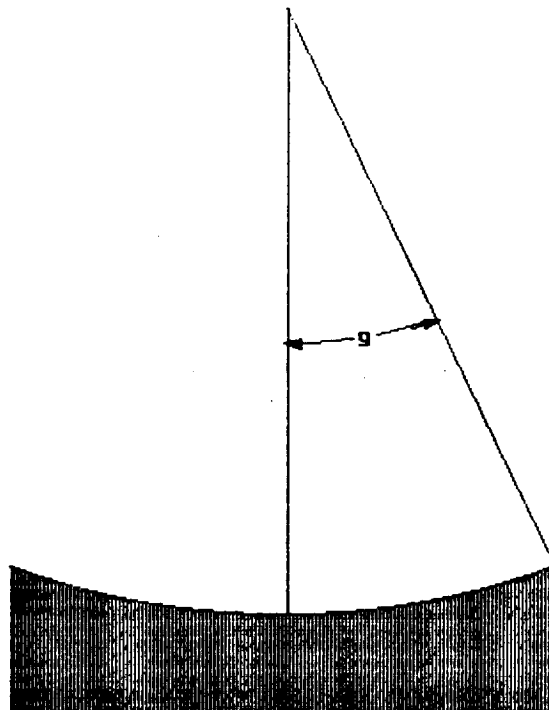


Figure 3B. Spherical Face of Polished Wire Bundle.



If a round bundle of wires (ideally hexagonal) is clamped, ground, and polished with a spherical surface as a concave mirror, the local slope of the surface is proportional to the radial location of each wire. The bundle is unclamped and the wires are slid past each other to be coplanar at their tipped edges.

The final step in making a phase scrambler plate is to heat the clamped bundle and press the array into a sheet of optical plastic to mold the final plate.

As a numerical example, consider the following parameters:

- 4" diameter lens ($A = 4$)
- image diameter is to be 2° angular width (for a 4° quad cell)
- phase scrambler plate plastic is acrylic ($n = 1.49$)

From the equations above,

- wire diameter $d = 0.0498"$ (approximately 18 gage)
- 5067 wires will be required to fill the 4" diameter aperture
- The maximum physical slope of sub-apertures at the edge of the acrylic plate is 2.041° (at the periphery of the 4" diameter)
- The radius on which the wire bundle is to be ground and polished is thus 28.061"
- The central concavity of the as-polished wire bundle is 0.030"

The concavity across a single wire face is approximately 0.062 micron ($\sim \lambda/10$). I.e., each sub-aperture is "optically flat" across its single face.

The maximum change in surface height across a single wire is 37.5μ , at the periphery. I.e., the prism tilt is large compared with the wavelength of light and the system will act as an array of geometric-optics prisms.

It is highly unlikely that any patches of the sub-aperture array will exhibit order, other than the center-to-center spacing. To reinforce this, the bundle of wires is re-stacked to "flatness" on a random, roughened surface such as sandpaper. Thus, the optical path of the principal ray through each sub-aperture of the phase scrambler plate will be different, and the diffraction patterns of the sub-apertures will add up in random phase, and average to a uniform amplitude.

MAPPING FUNCTION: CREATING A FOCAL SPOT OF ARBITRARY SIZE AND SHAPE

The arrangement described above has been shown to create a circular, uniformly illuminated impulse response (image of a point object) of large angular diameter, from an entire lens aperture. This results when the lens aperture is broken into many sub-apertures in random phase relationship, but where each sub-aperture is mapped into image plane in one-to-one correspondence, and where the diffraction-limited impulse response of each sub-aperture is large enough to exactly overlap those of contiguous sub-aperture according to the Sparrow criterion.



If a portion of the lens aperture is blocked, that corresponding portion of the image disc will disappear. Thus, this composite objective lens system has a peculiar property: the shape of the image of a point source is the same as the shape of the lens aperture. If the lens is masked to create a slit or rectangular pupil, then its image will be a geometrically similar slit or rectangle.

This is particularly valuable for the case of a quad-cell objective, for which the ideal impulse response is a square whose dimensions are equal to half the quad-cell diameter.

If a square aperture is to be constructed, then a simplified fabrication method may be used. This method--used in the Phase I experimental portion--does not use wires, polished to a spherical overall figure and used to emboss one side of the phase scrambler plate, as described earlier. Instead, 18-gage metal sheets were stacked on edge, clamped, ground and polished to form a cylindrical mirror (of the same radius of curvature as for the wire bundle). The sheets were unclamped, and the individual sheets moved past each other to be coplanar at their tipped edges. A plastic plate was thermally embossed on one side and then the other with the plates rotated at 90°. Each side of the finished phase scrambler plate bore prismatic strips whose apex angle increased toward the borders; in transmission the crossed strips in effect yielded square sub-apertures, with highly efficient use of the aperture surface.

This required, of course, that the star tracker be designed with a square aperture.

4.0 BREADBOARD THEORY

A breadboard optical system was designed to test and evaluate the use of the phase scrambler plate.

The breadboard consisted of an artificial star source, a quad-cell tracker, and the associated electronics.

4.1 Optics

In accordance with the Phase I proposal, a nested quad-cell concept was implemented. The optimal spot size on a quad cell is equal to half its width; any smaller and it falls completely on one leaf; any larger, and it falls off one or another edge as it moves. This is usually accomplished by defocus of the system, as illustrated for a Canopus tracker in Figure 4. The location signal as the central spot moves (e.g., from left to right) is highly nonlinear: the output signal is the convolution of an edge with a Gaussian of revolution, as illustrated in Figure 5.

The phase scrambler plate was developed to permit a large (2°) star image to be formed by a conventional lens, with minimum light loss. The use of such a uniformly illuminated square spot as illustrated in Figure 6 permits a very linear output, as shown in Figure 7.

Since we have gone to considerable length to create a large (2° square) focal spot, the objective lens need not be of high quality. In the case of the breadboard, a plastic Fresnel lens (254 mm focal length) proved quite satisfactory.

The aperture was set at 100 mm square. This exceeds that of earlier star trackers, yet the lens is quite light weight.



ORIGINAL PAGE IS
OF POOR QUALITY

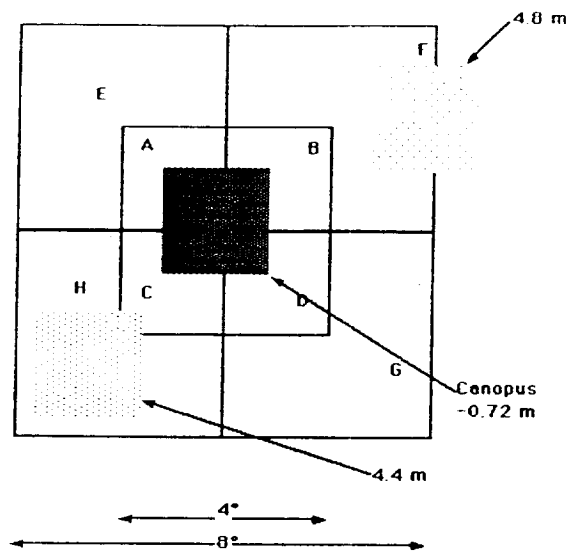


Figure 6A. Square Uniform-Irradiance Star Images on Square Quad-Cell Detectors.

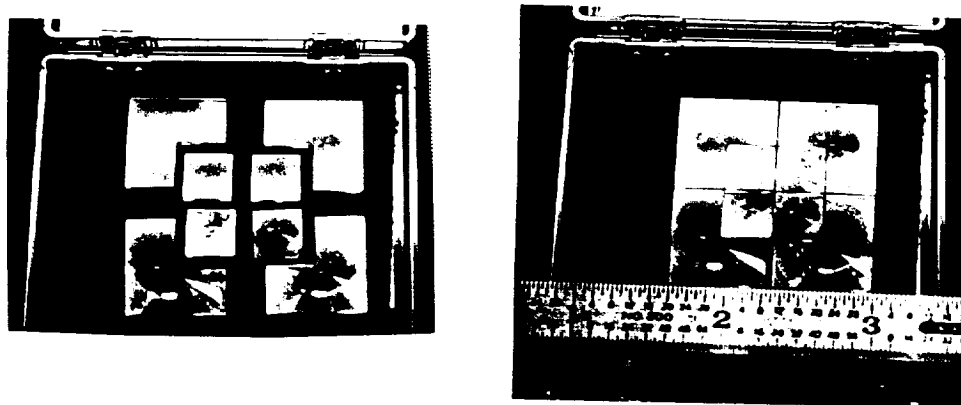


Figure 6B. Actual Quad-Cell Lenslet Array.

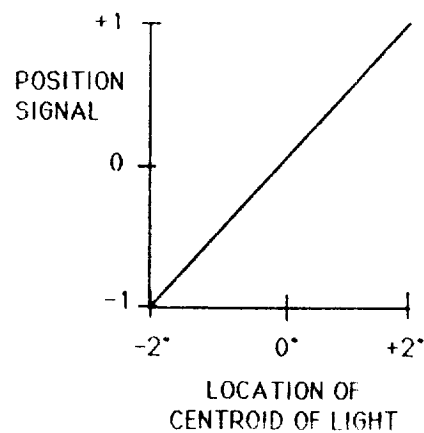


Figure 7. Linear Quad-Cell Signal Response Using Square, Uniformly Illuminated Spot.

4.2 Detectors

An integrated (single-crystal) detector array, schematically sketched in Figure 6, was not built in this Phase I effort.

Rather than a custom detector array to dissect the image plane, an array of lenses was assembled to replace the detector array, and 8 images of the objective lens pupil were relayed onto a checkerboard detector plane which is shown in Figure 8.

Interestingly enough, this does not compromise signal/noise.

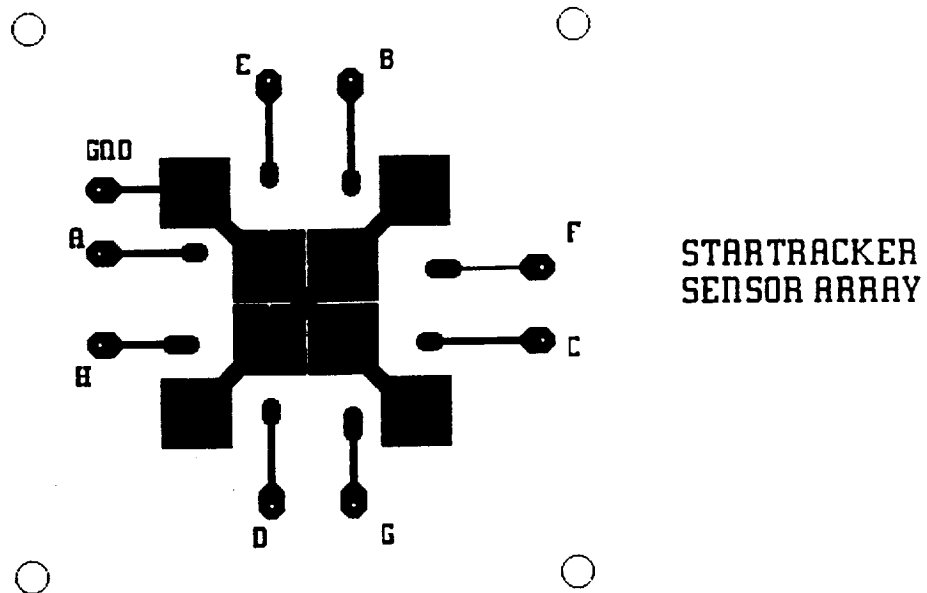


Figure 8. Checkerboard Array of Detector Chips, Board Mounted.

With the simple classical radiometer of Figure 9, the field of view (FOV) is related to the detector width and the focal length f_1 : $FOV = 2 \text{ Arctan} (d/2f_1)$.

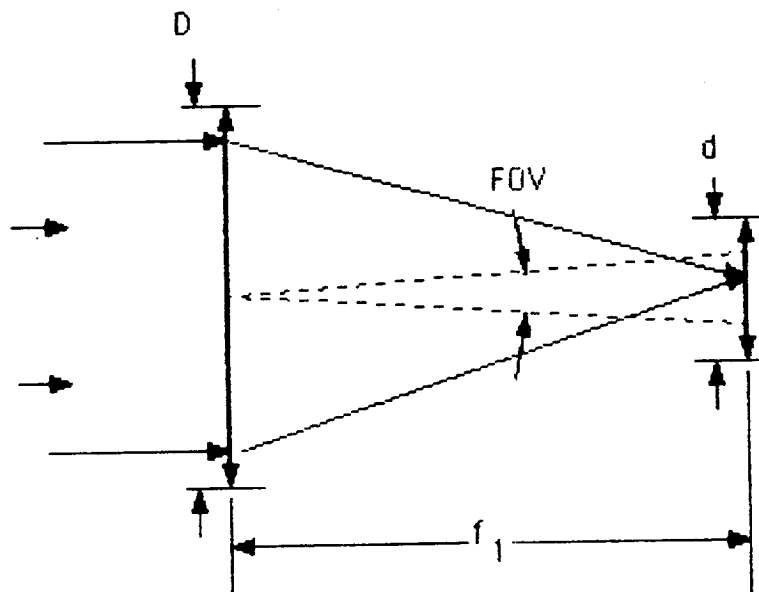


Figure 9.



1. By inspection of the sketch, detector diameter $d \sim (\text{FOV } f_1)$.
2. But, $f_1/D = F\#$ of the objective lens.
3. Hence, $D/d = 1/(F\# \text{ FOV})$. But detector noise is proportional to the square root of the resistance of the detector, i.e., proportional to its diameter d ; the signal is proportional to the area of the objective lens, or the square of its diameter D .
4. Multiplying both sides by D :

$$\text{Signal/noise proportional to: } D^2/d = K \frac{D}{F\# \text{ FOV}}$$

where K = a constant of the system.

Such a conventional radiometer would have required direct construction of a nested quad-cell array. As the breadboard was actually designed, a relay lens array was placed at the focus of the objective lens to dissect the image in the pattern of Figure 8. Figure 10 sketches the optical layout.

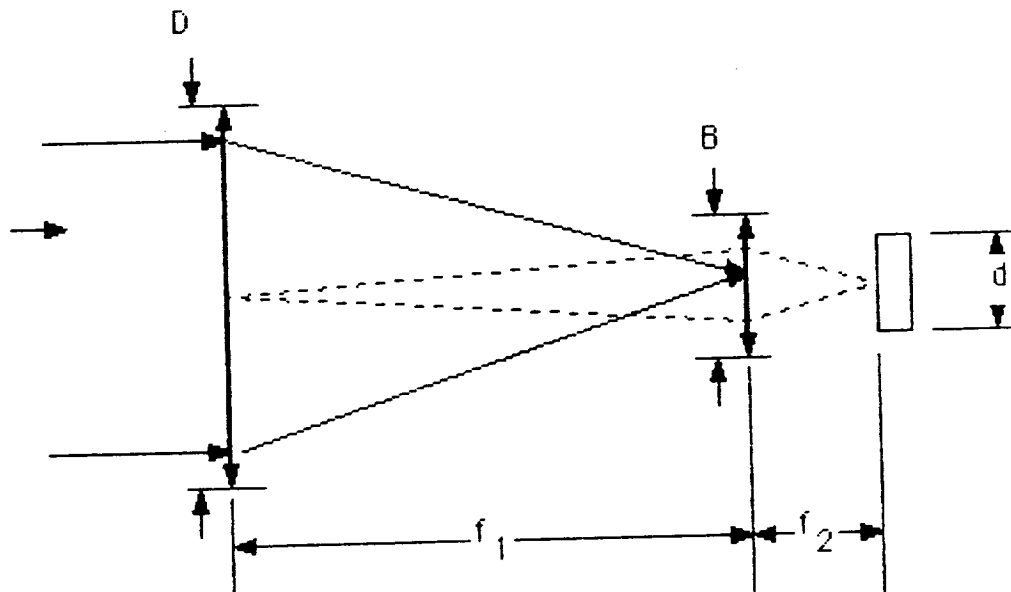


Figure 10.



1. The image-segmenting lens has a required diameter $B = (\text{FOV})(f_1)$, where FOV is the field of view covered by the radiometer without vignetting.
2. Its focal ratio is $F\# = f_2/B$.

The magnified image of the objective lens aperture D on the detector is: $d \sim D f_2/f_1$.

$$\text{so: } d = D F\# B/f_1$$

$$\text{so: } d = D F\# \text{FOV } f_1/f_1 = D (F\# \text{FOV})$$

But detector noise is proportional to the square root of the resistance of the detector, i.e., proportional to its diameter d ; the signal is proportional to the area of the objective lens, or the square of its diameter D .

$$D/d = 1/(F\# \text{FOV})$$

3. Multiplying both sides by D and rearranging, we have:

$$\text{Signal/noise (proportional to } D^2/d) = K \frac{D}{F\# \text{FOV}}$$

where $K = \text{a constant of the detector}$.

4. The FOV is fixed by other analysis, e.g., at 8° and $F\# \sim$ a realistic minimum of 1. Thus, the system signal/noise is independent of the focal lengths of the components, but is proportional to the diameter D of the objective, and is equivalent for both radiometer designs.

The lenslet array, made in the pattern of Figure 6, produces 8 aerial images of the objective lens. A separate detector chip is located at each of these images, to sum the radiation passing through its respective lenslet.

The active area of the detector array is shown in Figure 8. The ground plane is shown, all interconnected. Individual detector chips were glued in checkerboard pattern, at locations calculated by geometric raytracing to be at the aerial images.

The $F\#$ of the relay lenslets was actually faster than 1: on the order of $F/0.8$. Thus, the signal/noise of the breadboard optical system is actually higher than it would be were the detectors directly illuminated.

4.3 Electronics

Refer to Figure 11, Block Diagram, for the following discussion.

The detector outputs are connected to four pre-amplifiers. Switches are provided at the detector outputs so that only an inner set of detectors provides signals to the pre-amplifiers or



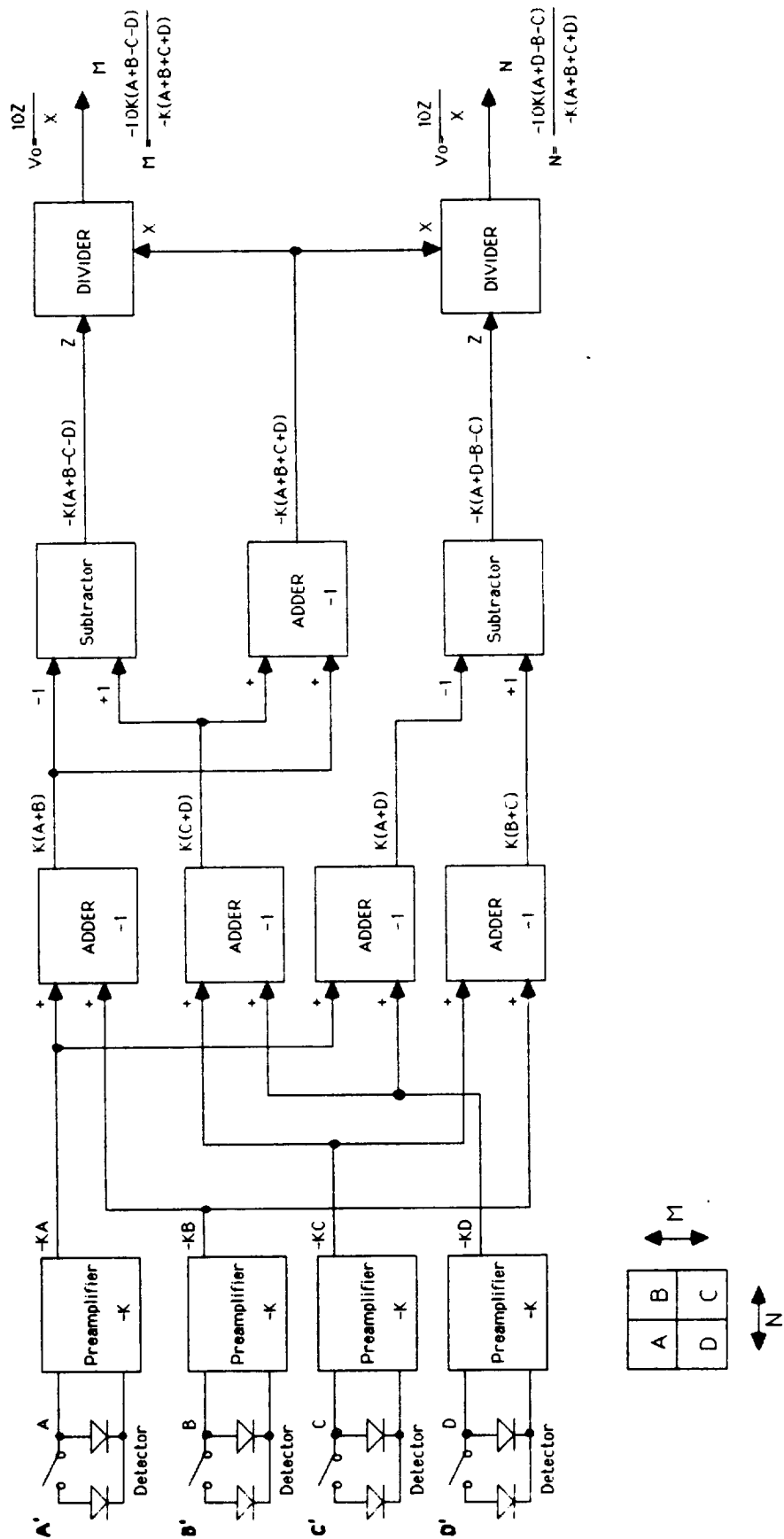


Figure 11. Amplifier Block Diagram.



both inner and outer detectors combine to provide signals to pre-amplifiers.

The devices used for pre-amplifiers are chopper stabilized, low-noise integrated circuits having very low dc drift. The amplifiers are operated as dc-coupled transimpedance amplifiers with the gain set at 1 volt of output for 10^{-10} amperes of input.

Refer to Figure 6 for image location and Figure 8 for the detector arrangement. If a pre-amplifier gain is designated as K and all pre-amplifiers are assumed to have equal gain, then the output of the pre-amplifier connected to the "A" detector will be KA, the one connected to the "B" detector will be KB, etc.

A circuit is connected to the pre-amplifier outputs that performs summing, subtracting, and dividing functions so that two outputs are generated having their amplitudes and signs describe the position of the light falling on the detector array. Four adders sum the pre-amplifier outputs in pairs on each side of the center lines of two detector array axes. Two subtracters follow which compute the differences of the opposing pairs of signals to develop the basic offset signals. An adder sums all four pre-amplifier outputs, and dividers produce the ratio of the different signals and the total signal. This latter computation provides a correction of the scale factor as a function of light level.

The "M" output is:

$$\frac{10 (A + B - C - D)}{A + B + C + D}$$

The "N" output is:

$$\frac{10 (A + D - B - C)}{A + B + C + D}$$

4.4 Artificial Star Source

An artificial star source was made, using a large fresnel lens corrected for spherical aberration.

The angular width of the star should be small compared to the detail of the star tracker image. The collimating lens was chosen to be 24" focal length, 10.5 x 10.5 inches square. A 0.020-inch fiber optic was used as the star source, illuminated by a commercial quartz-iodine vapor source.

The angular width of the collimated point source is 2.3% of the 2° beam width created in the phase scrambler plate, and is deemed adequately small.

The fiber optic is potted in a tubulation extending from the rear of the star source housing, and may be refocused and locked at the lens' nodal point.

5.0 EXPERIMENTAL APPARATUS

The experimental apparatus consist of an artificial star source, a phase scrambler element, and star tracker. The apparatus was mounted on an optical bench with a two axis computer-operated gimbal system to perform testing.



5.1 Opto-Mechanics

ARTIFICIAL STAR SOURCE

The artificial star source consists of a 24" long light-tight housing with a 12" x 12" Fresnel collimating lens, a fibre optic bundle together with an illumination source. A single optical fibre was illuminated to provide an adequate "star" image. The star source is seen in Figure 12.

PHASE SCRAMBLER ELEMENT

The experimental phase scrambler element consisting of a series of prismatic surfaces at right angles, made by hot impression forming an acrylic material using the single male die-set described below, was used to make the two (orthogonal) phase scrambler prism arrays.

- *Die-set*

The die-set, shown in Figure 13, consists of multiple plates (.0475" nominal thickness) stacked in compression between two 0.5" sideplates. A negative radius, with the cylindrical axis parallel to the length of the plates, was computer numerically controlled (CNC) generated in the edges of the clamped assembly of plates and hand polished. An equivalent male (positive radius) was made using the same CNC program. Impressions of the negative radius was cast in dental cement and then used as radius polishing blocks. After polishing, the compression was relieved on the plate stack and the negative radius (the prismatic edges of the plates) made coplanar by allowing individual plates to settle on a flat surface to create an impression surface with a "saw-tooth" pattern. The plate stack was again put in compression and mounted on top of the male pattern to form the die-set shown in Figure 13.

- *Manufacture*

The phase scrambler element was manufactured using the single-sided male die element described above.

The die-set was put on the lower platen of the hot press and heated to a temperature slightly in excess of the forming temperature of the acrylic material (approximately 375°F). The acrylic material was fastened to a flat glass plate and placed on top of the heated die and placed under pressure at approximately 80-100 psi.

After the first impression, the element was rotated 90° and turned over to make a second impression on the opposite side so that the prismatic surfaces on opposing faces of the PSP are at right angles. The finished PSP element is shown in Figure 14.

A second set of elements was made using an alternate manufacturing method which consisted of casting two replications in a clear polyester compound. These were then





Figure 12. Experimental Setup.



Figure 13A. Steel Plate Die Set.

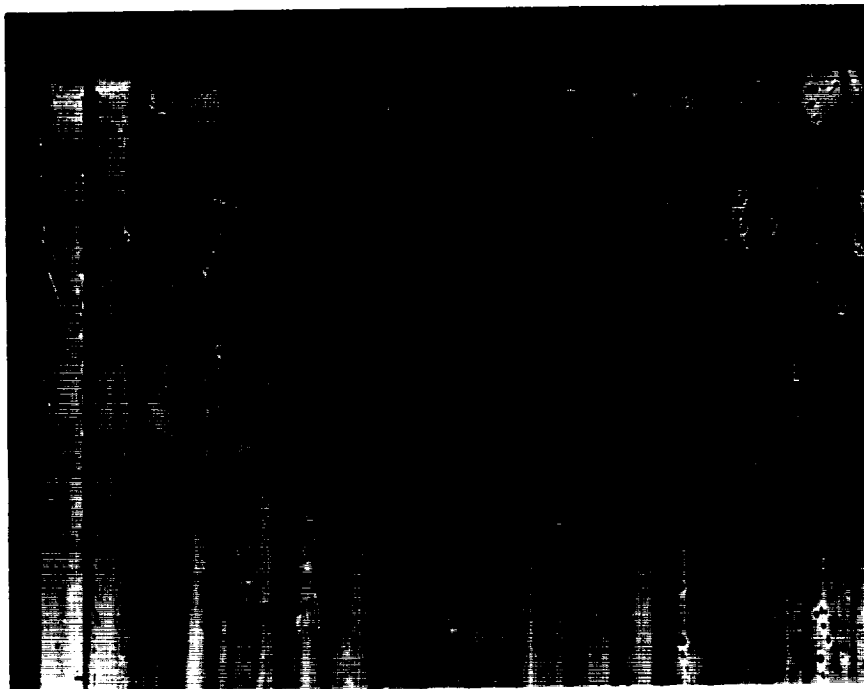


Figure 13B. Enlargement of a Section of Figure 13A.



Figure 14A. Phase Scrambler Half-Element.



Figure 14B. Enlargement of a Section of Figure 14A.

ORIGINAL PAGE
BLACK AND WHITE PHOTOGRAPH

made into a window with the replicated prismatic surfaces facing each other at right angles.

STAR TRACKER

The star tracker itself consists of a primary (Fresnel) lens, the phase scrambler element, described above, a lenslet/detector array plate (which is a pre-focused assembly), fastened to an adjustable slide, and a pre-amplifier array for the detectors. These are shown disassembled in Figure 15. The nested quad-cell lenslet array (schematically shown in Figure 6) is shown in Figure 16, with the preamp board behind it. A side view of the lenslet array in Figure 17 also shows the assembled detector array sketched in Figure 8. After installing the primary lens in the housing, the lenslet/detector array slide is installed, focused and secured, the phase scrambler is then installed between the primary lens and the array plate. These elements are all contained in a light-tight closed housing.

- *Test Set-up*

The following test set-up criteria was established for performing the experiment:

- a) The centerlines of the star source and tracker should be coincident.
- b) The star tracker breadboard should be moveable in pitch and yaw about the objective lens' first nodal point. It was mounted on a motorized pair of orthogonal rotary bases as shown in Figure 12 and 18. These were positioned by computer to within 0.001° .

This was accomplished by drilling a hole in the tracker baseplate at the above-described point and mounting the plate on a pin, using spacers, at the rotational centers of the 2-axis mechanism. The plate was secured so that the angular motion required was done using the 2-axis mechanism. The rotary table providing motion about the vertical axis is mounted on a goniometer which provide motion about the horizontal axis.

The star source was fixedly mounted on a adjustable leveling plate, adjusted and aligned until its centerline was coincident with the tracker.

5.2 Electronics

Pre-Amplifier. The pre-amplifier design uses a chopper stabilized integrated circuit amplifier. The noise contribution of the amplifier is sufficiently small to allow a good signals-to-noise ratio using the optical components and the bandwidth of the experiment. The transimpedance of the pre-amplifier was set by an inverse feedback network. The gain used was 1 volt output for 10^{-10} ampere input. The bandwidth is set as .72 Hz by a capacitor across the feedback network. The chopper stabilized amplifier provided extremely low voltage and current drift. The output signal levels range from zero to four volts.



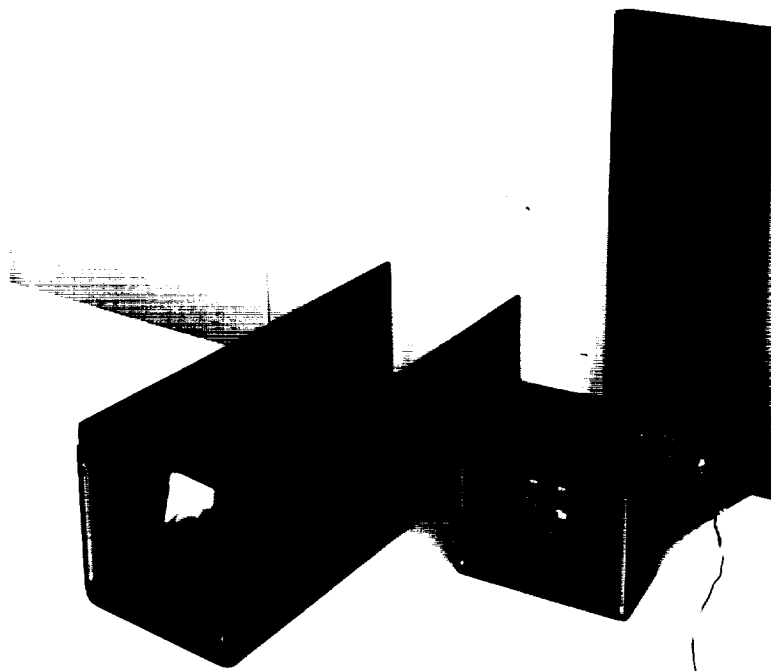


Figure 15. Star Tracker, Disassembled.

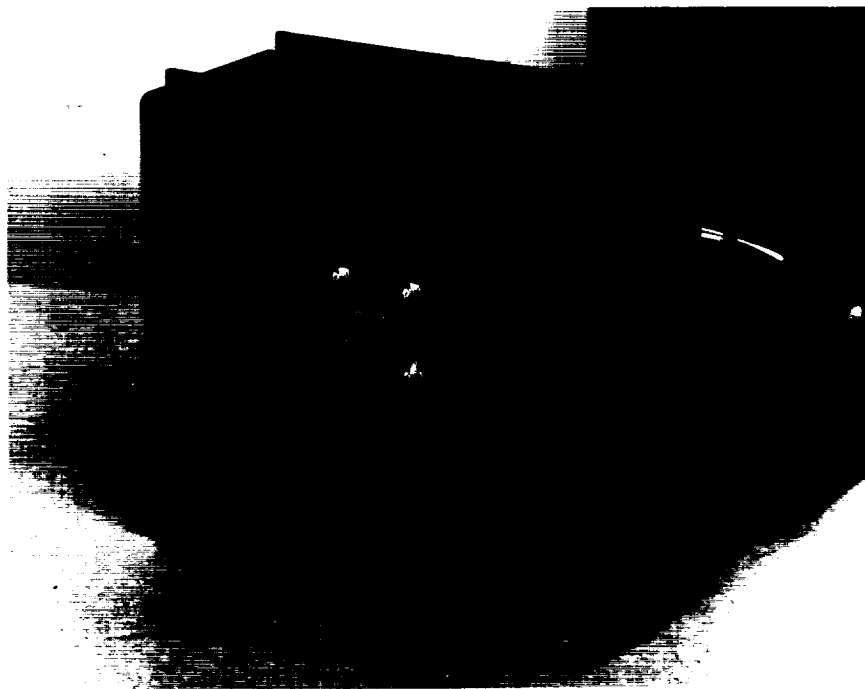


Figure 16. Nested Quad-Cell Detector Subsystem.

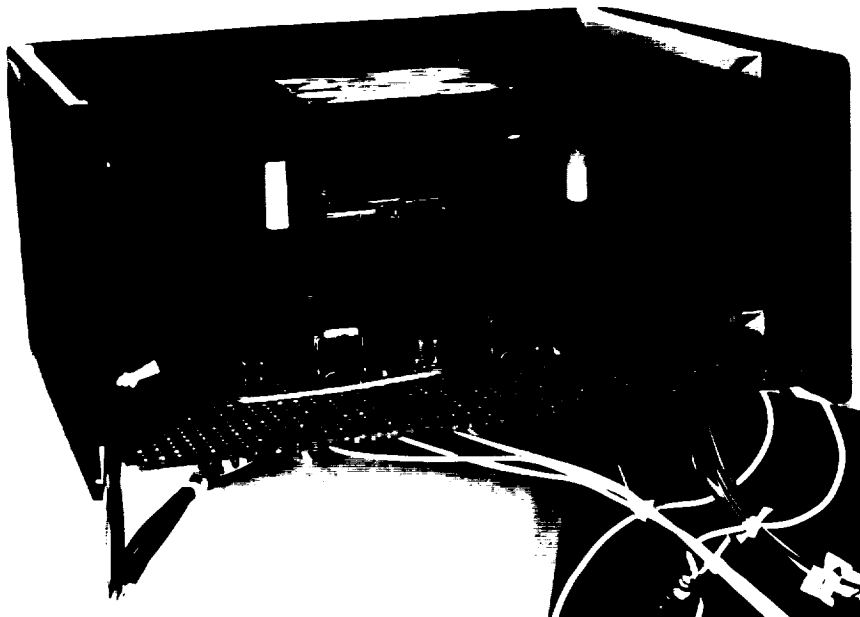


Figure 17. Detection Subsystem:

- Image Dissecting Lenslet Array
- Detector Checkerboard Array
- Pre-Amp Circuit Board



Figure 18. Star Tracker, Rotated 90° on Motorized Base.

Position Computation. The input signal levels were nominally in the range of several volts. At this input level, drifts on the order of a millivolt provided good performance. The gains of all adding and subtracting elements were set a unity. The division functions were performed by using four quadrant analog multiplier integrated circuits with the feedback circuit connected to realize the division function. Trim adjustments were provided to allow gain, axis scale factors, and initial offset adjustments.

Schematics of the pre-amplifier and the position computation circuit are shown in Figure 19 and Figure 20. Figure 17 is a photograph of the pre-amplifier circuit board. Figure 21 shows the position computation assembly on the left. It and other related electronics are shown sitting on top of the gimbal positioning drives.

6.0 EXPERIMENTAL RESULTS

The experiments amply confirmed the utility of the phase scrambler plate, subject to the limitations of the crude nature of the fabrication process.

The PSP showed the desired variable-prism angle across its face. The best one still showed considerable scratch, dig, and bubble, but converted a point star image into an essentially uniformly illuminated square image.

6.1 Image Analysis

The star tracker breadboard detector was traversed by moving the star image across the field of view in both the defocused (circular Gaussian) and the focused PSP state.

Photographs were taken of the image. Conventionally, a quad-cell star tracker achieves the enlarged spot by defocussing the image as is shown in Figure 22A. Off axis, the output is highly non-linear corresponding to the plotted results shown in Figure 23.

In contrast, the PSP yielded a uniformly illuminated square focal spot, as shown in Figure 22B. Even with the hand-made first model of the PSP, the improved quad-cell tracker breadboard yielded a much more linear output, as shown in Figure 24.

In addition, an objective lens system has been developed, for which the image size and shape remain constant across the FOV and over a wide temperature range. This lens system is superior to conventional optics that are used to defocus star images in order to obtain image spread to accommodate pointing and tracking.

7.0 CONCLUSIONS AND RECOMMENDATIONS FOR FURTHER WORK

The successful demonstration in Phase I of the first phase scrambler plate opens new opportunities for the use of quad cells and quad-cell like (e.g., CCD) sensors in metrically accurate star sensors.

The PSP may be used to methodically modify the impulse response of any lens system. For example, a telescope may be given a uniformly illuminated focal spot in the shape of a rectangle, line, cross, circle, or annulus by simply modifying the equations by which the PSP is made.



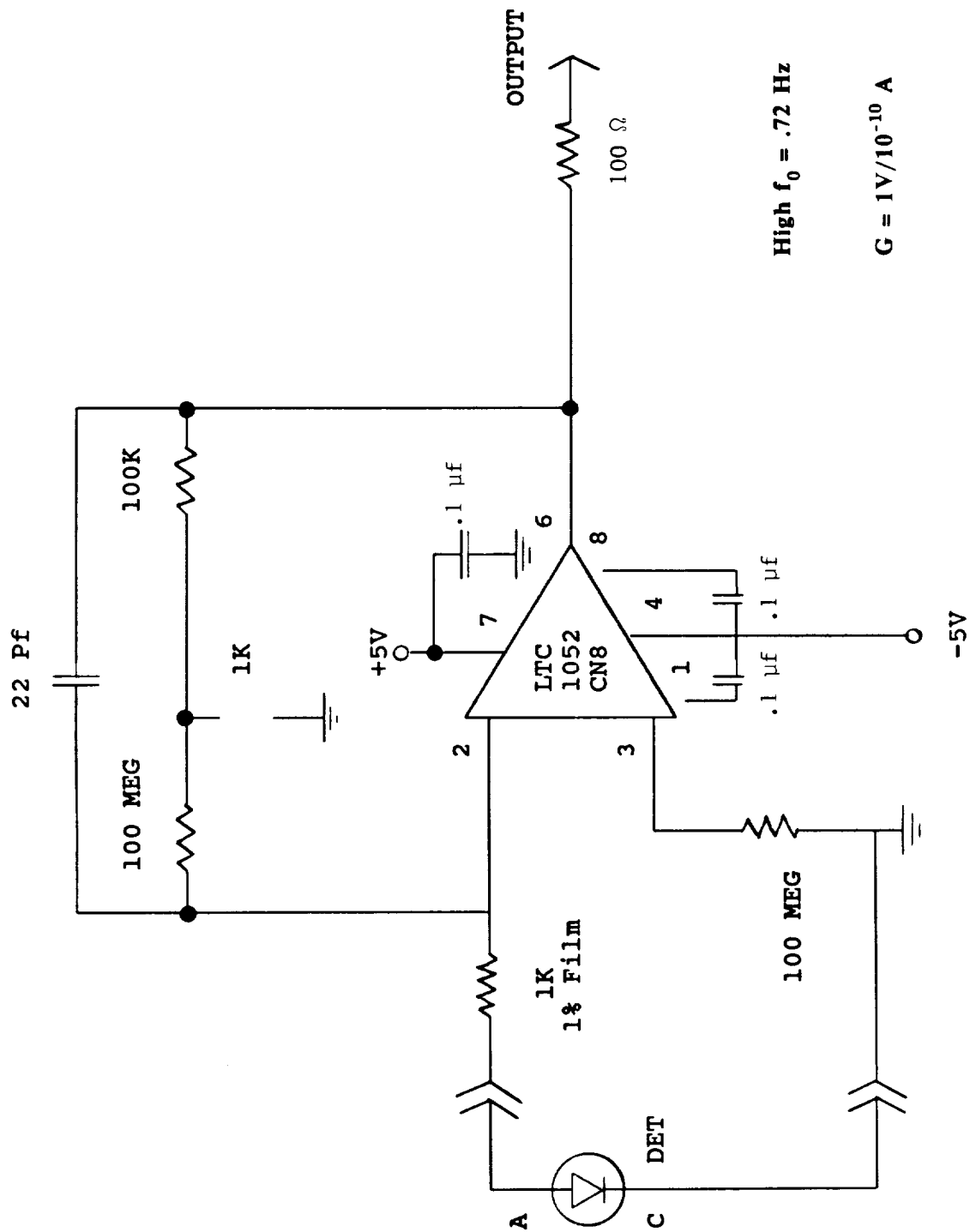


Figure 19. Star Tracker Pre-Amplifier, DC-Coupled.



ORIGINAL PAGE IS
OF POOR QUALITY

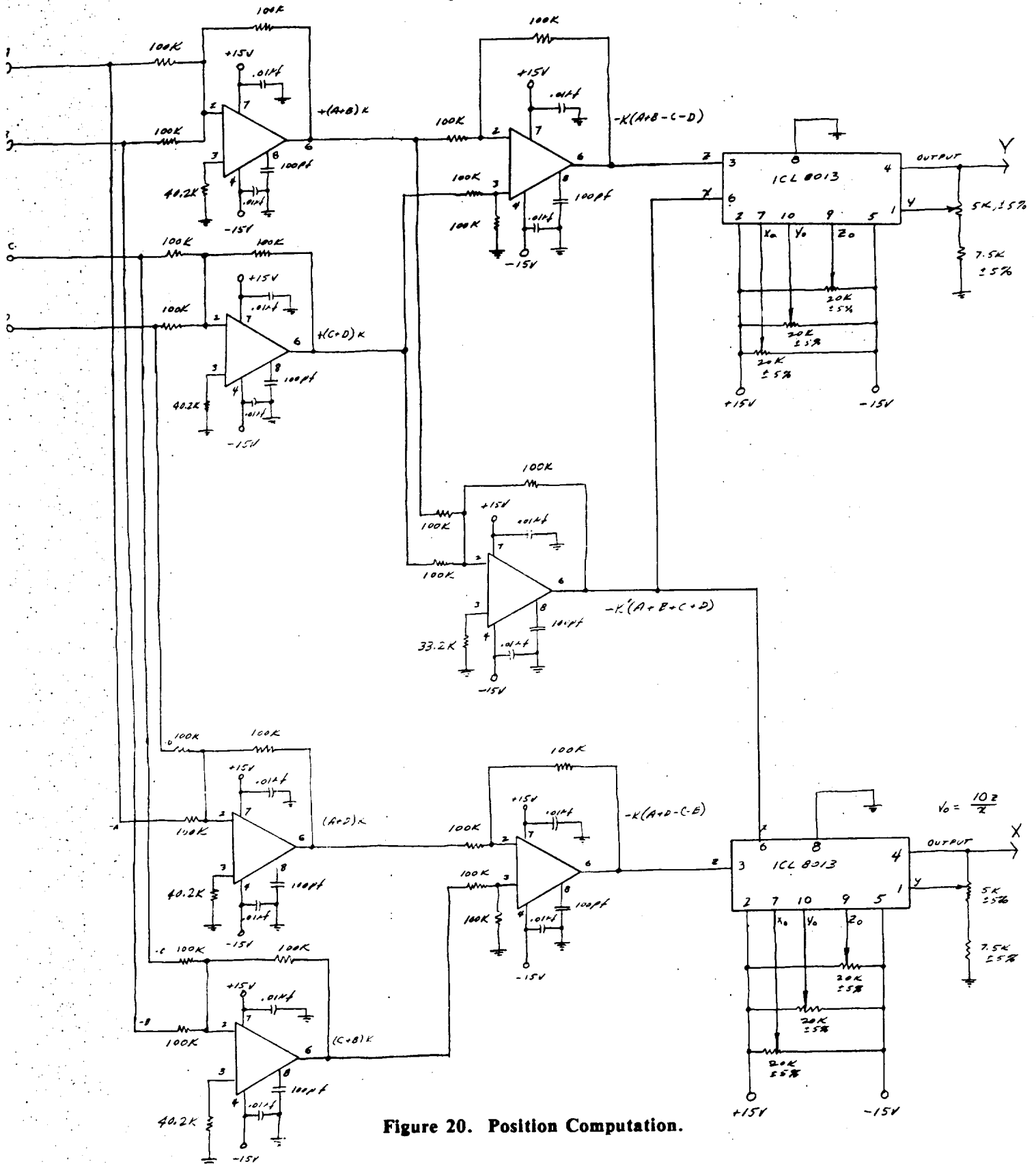


Figure 20. Position Computation.

NOTE: OP Amps LM 308N

Resistors 1%, except as marked.

ORIGINAL PAGE
BLACK AND WHITE PHOTOGRAPH

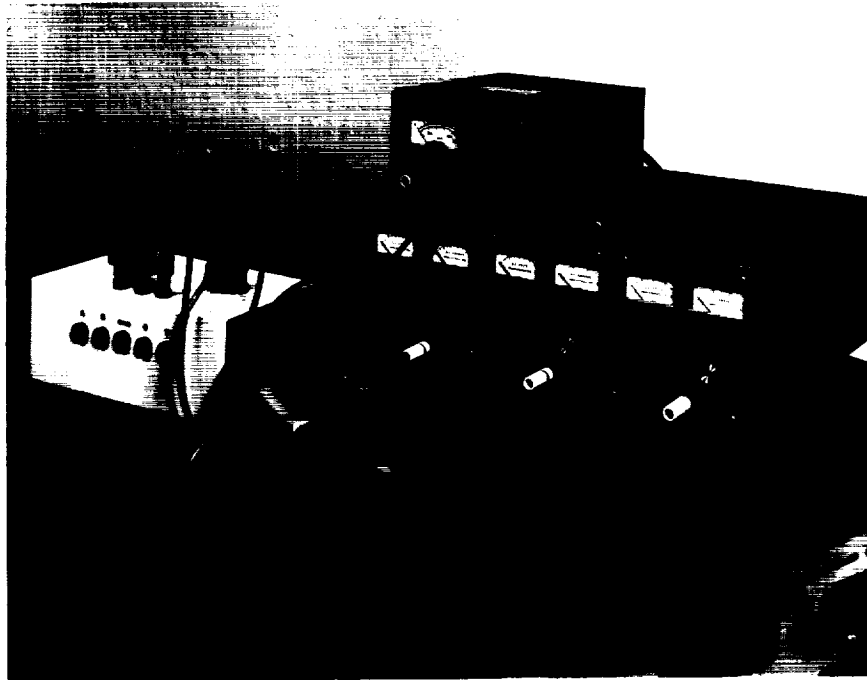


Figure 21. Electronics Controls

ORIGINAL PAGE IS
OF POOR QUALITY

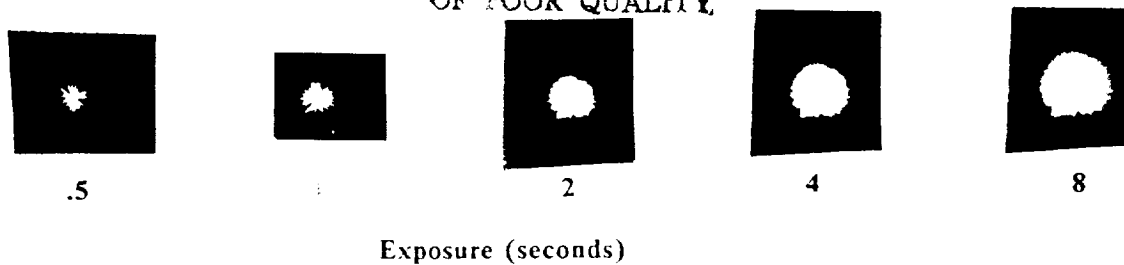


Figure 22A. Round, Pseudo-Gaussian Star Images Created by Defocussing to 2° Diameter.

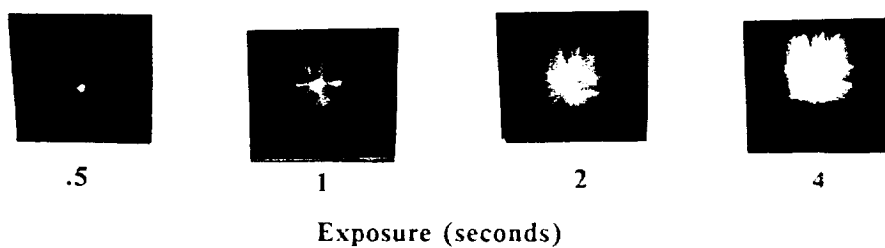


Figure 22B. Square Uniform-Irradiance Star Images, Created at the Focal Plane by the Breadboard PSP.

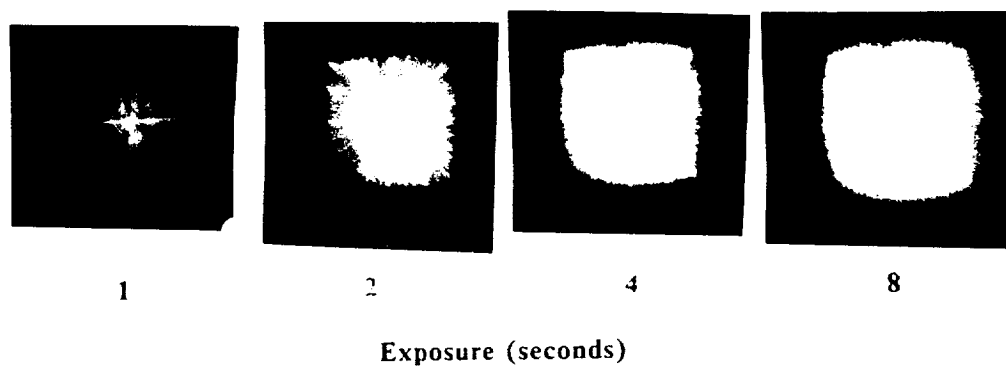


Figure 22C. 2X Enlargement of Square Star Images. Note Uniformity of Illumination.

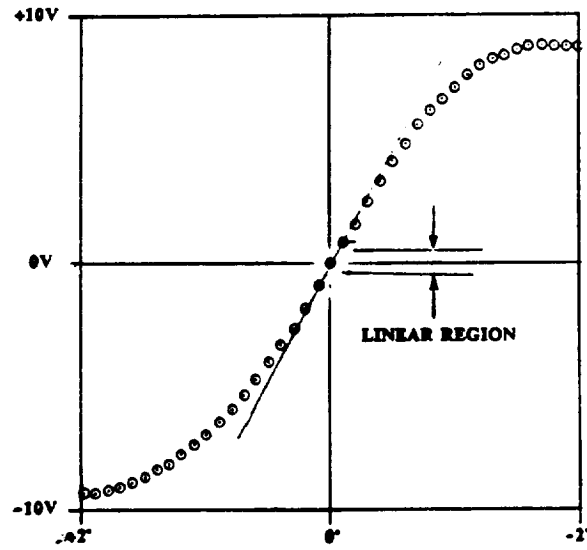


Figure 23. Defocussed (Circular, Pseudo-Gaussian) Image.

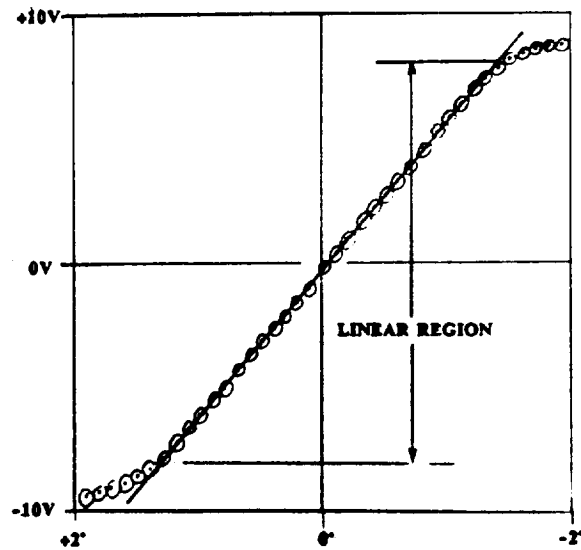


Figure 24. Focussed Square-Spot Image With Experimental PSP.



This may find applications in surveying instruments, weapon sights, stellar spectrometry, or of course in the original application: quad cell star trackers.

In Phase I, the PSP and the optics were made of acrylic for convenience. In a next development phase, they should be fabricated and tested in glass.

The detector area is necessarily large, and consequently noisy. Either it should be cooled, or an image-intensifier pre-amplifier should be used to increase the instrument sensitivity.

Quantic recommends that a flightworthy model of the star tracker be made and tested as a logical continuing effort.

This star tracker innovation is not an unproven jump into the unknown, but a new combination of present art. The components are readily available or are easily fabricated from off-the-shelf materials. Moving directly to fabrication and testing of a flight model in a Phase II SBIR program is a logical extension of the effort.

